Ionothermal Synthesis of BiOCl Nanostructures via a Long-Chain Ionic Liquid Precursor Route

ARTICLE *in* CRYSTAL GROWTH & DESIGN · MAY 2010

Impact Factor: 4.89 · DOI: 10.1021/cg900940s

DOI: 10.1021/cg1006567

CRYSTAL GROWTH & DESIGN Article

2010, Vol. 10
4449–4455

Shape-Controlled Synthesis of Metal Carbonate Nanostructure via Ionic Liquid-Assisted Hydrothermal Route: The Case of Manganese Carbonate

Xiaochuan Duan, Jiabiao Lian, Jianmin Ma, Tongil Kim, and Wenjun Zheng*

Department of Materials Chemistry, Key Laboratory of Advanced Energy Materials Chemistry (MOE), College of Chemistry, Nankai University, 94 Weijin Road, Tianjin 300071, P. R. China

Received May 18, 2010; Revised Manuscript Received August 24, 2010

ABSTRACT: The $MnCO_3$ hollow microspheres and nanocubes have been successfully synthesized via an ionic liquid-assisted hydrothermal synthetic method. The samples are characterized by X-ray diffraction (XRD), Fourier transform infrared spectroscopy (FT-IR), field emission scanning electron microscope (FE-SEM), transmission electron microscopy (TEM), and high-resolution transmission electron microscopy (HRTEM). Our experimental results demonstrate that the $MnCO_3$ hollow microspheres are obtained by self-assembly under the driving force of Ostwald ripening process. Moreover, we found that the sizes and morphologies of the crystals depended on the concentration of the ionic liquid, and we obtained the $MnCO_3$ nanocubes formed by ordered aggregation of nanoplates with high concentration of [bmim][Cl]. The effects of [bmim][Cl] on the formation of the $MnCO_3$ have been investigated systematically. This method is expected to be a useful technique to prepare other metal carbonates for controlling the diverse shapes and sizes.

1. Introduction

Room temperature ionic liquids (RTILs), a family of low-temperature molten salts composed of organic cations and inorganic or organic anions,[1] have found applications in various fields such as organic chemical reactions,[2] catalysis, extractions,[3] and electrochemistry.[4] In recent years, significant progress has been made in controlling the morphology and chemical and physical properties of inorganic nanocrystals using the ionothermal synthesis and ionic liquid-assisted synthesis.[5] Because in view of today's environmental concerns, RTILs are considered as "green" solvents as a new class of compounds for replacement of conventional organic solvents due to their high fluidity, low melting temperature, and extended temperature range in the liquid state, air and water stability, low toxicity, nonflammability, high ionic conductivity, ability to dissolve a variety of materials, and importantly no measurable vapor pressure. ILs can act as new reaction media for reactants and morphology templates for the products at the same time, which enables the synthesis of inorganic materials with novel or improved properties. Novel nanostructures could be fabricated by selecting suitable IL reaction systems. For instance, in the previous work, our group has reported the synthesis of pure rutile and rutile-anatase composite TiO_2 nanoparticles,[6] α-Fe_2O_3 with various morphologies,[7] a series of shape-controllable ZnO nanocrystals,[8] ZnSe hollow nanosphere,[9] and γ-Al_2O_3 nanostructures[10] using different ionic liquids.

Metal carbonates have been intensively investigated in recent years because of their abundance in nature and also their important industrial applications in paints, plastics, rubber, and paper. Moreover, the metal carbonates (e.g., $CoCO_3$ and $MnCO_3$) are often used as solid precursors to synthesize their respective nanostructured metal oxides through chemical/thermal conversion.[11] However, to the best of our knowledge, the synthesis of metal carbonates using ionic liquids is rare. Hollow $CaCO_3$ spheres were synthesized in water/[HMim]-[BF_4] emulsions using $CaCl_2$ as the precursor.[12] Shan and co-workers prepared strawlike $SrCO_3$, $CaCO_3$, and $MnCO_3$ bundles using 1-methyl-3-pentylimidazolium pyruvate.[13] More recently, Wang and co-workers investigated the calcium carbonate ($CaCO_3$) crystallization controlled by imidazolium based ionic liquids.[14] However, metal carbonates prepared in these studies all have relatively big grain sizes and the preparation of monodispersed metal carbonate nanoparticles using ionic liquids virtually has not been reported.[15]

In this study, we report our recent efforts on the synthesis of $MnCO_3$ on a lager scale using an ionic liquid (1-*n*-butyl-3-methylimidazolium chloride, [bmim][Cl]) assisted process. Our experimental results demonstrate that the $MnCO_3$ hollow microspheres are obtained by self-assembly under the driving force of Ostwald ripening process in which larger crystal particles are essentially immobile and keep growing while smaller ones are undergoing mass relocation through dissolving and regrowing.[16] Moreover, we found that the sizes and morphologies of the crystals depended on the concentration of the ionic liquid, and we obtained the $MnCO_3$ nanocubes formed by ordered aggregation of nanoplates with high concentration of [bmim][Cl]. There are three significant features in this work: (i) The formation of $MnCO_3$ hollow microspheres may represent a new example of Ostwald ripening mechanism-based formation of inorganic hollow structures since application of the Ostwald repening mechanism was proposed for the first time in the synthesis of TiO_2 hollow nanospheres reported by Zeng et al.[17] (ii) Excellent studies on how ionic liquids influence the morphology have been carried out, and great achievements have been made. However, it seems to be that little work has been focused on the comprehensive consideration of the role of ionic liquids, just simple as a soft template or a capping agent, which is not enough to show the advantages of ionic liquids. Herein, we systematic report the different role of ionic liquids with different concentration and how to influence the morphology. (iii) As far as our knowledge, it is rare to report the preparation of small size

*To whom correspondence should be addressed. Phone: +86-022-23507951. Fax: +86-022-23502458. E-mail: zhwj@nankai.edu.cn.

Published on Web 09/08/2010

Scheme 1. 1-*n*-butyl-3-methylimidazolium chloride

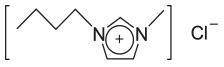

(~200 nm) manganese carbonate nanostructures using ionic liquids, which is highly expected that such a simple and mild route could also to be extended to prepare other metal carbonates MCO_3 (M = Sr, Ca, etc.) with small size nanostructures.

2. Experimental Section

All the reagents were analytical grade and used without further purification. The ionic liquid 1-*n*-butyl-3-methylimidazolium chloride ([bmim][Cl]) was prepared according to the literature[18] (see the Supporting Information), and its general structure was shown in Scheme 1.

2.1. One-Step Synthesis of the $MnCO_3$ Hollow Microspheres and Nanocubes. In the typical synthesis procedure, 0.5 mmol of $MnCl_2 \cdot 4H_2O$ was put into deionized water under stirring to form a homogeneous solution. Subsequently, 0, 0.2, 2, 5, 8, 10, 12, and 14 mL of the [bmim][Cl] was added into the above homogeneous solution under continuous stirring, respectively. Then 2.5 mmol of NH_4HCO_3 was added into the above solution under continuous stirring. After stirring for 20 min, the total solution was transferred into a stainless-steel autoclave with a capacity of 20 mL, sealed and heated at 120 °C for 12 h. When the reaction was completed, the autoclave was cooled to room temperature naturally. The resultant product was collected and washed with deionized water and anhydrous ethanol for several times until the solution was neutral. The final red product was dried in a vacuum at 80 °C for 3 h. The synthetic conditions for preparing some typical samples are summarized in Table 1.

2.2. Characterizations of Samples. The products were characterized by XRD, FTIR, SEM, TEM, and HR-TEM measurements. XRD measurements were performed on a Rigaku D/max 2500 diffractometer with Cu Kα radiation (λ = 0.154056 nm) at V = 40 kV and I = 150 mA, and the scanning speed was 8°/min. The FTIR spectra of the samples were conducted at room temperature with a KBr pellet on a VECTOR-22 (Bruker) spectrometer ranging from 400 to 4000 cm^{-1}. Morphology observations were performed on a JEOL JSM-6700F field emission scanning electron microscope (FE-SEM). TEM and HR-TEM images were recorded with a Tecnai G2 20S-Twin transmission electron microscope operating at an accelerating voltage of 120 kV.

3. Results and Discussions

3.1. Structure Characterization. The phase and purity of the as-obtained $MnCO_3$ nanocubes and microspheres were characterized by powder XRD measurements, as shown in parts a and b of Figure 1, respectively. In both patterns, it is evident that all the diffraction peaks can be perfectly indexed to the rhombohedral structure of $MnCO_3$ with lattice constants a = 4.772 Å and c = 15.651 Å, which are consistent with the reported values (JCPDS Card 83-1763). To reveal the chemical composition and bonding situation of $MnCO_3$ crystals, the FT-IR investigation has been carried out. Figure S1b of Supporting Information presents a typical FT-IR spectrum of the as-prepared $MnCO_3$ samples. The bond at around 3375 cm^{-1} is assigned to the stretching vibration of the O−H group of surface adsorbed molecular water and hydrogen bond O−H. The presence of CO_3^{2-} in the as-prepared $MnCO_3$ sample is evidenced by its fingerprint peaks of D_{3h} symmetry at 1477, 865, and 744 cm^{-1}, which are assigned to vibrational modes of $\nu_3(E')$, $\nu_2(A_1'')$, and $\nu_4(E'')$, respectively, according to normal modes of vibration of planar CO_3^{2-}; the peak located at 2509 cm^{-1} is also commonly associated to a vibrational mode of carbonate anion. The weak peak at 1810 cm^{-1} is attributed to an overtone or combination band composed of contributions from the combination of some vibrational modes of the carbonate groups and divalent metal ions.[11b,19] In addition, the results of C, H, N elemental analysis display that no [bmim][Cl] obviously resides at the samples after washing with distilled water and anhydrous alcohol for several times.

Table 1. Summary of the Experimental Parameters and Their Corresponding Morphologies of $MnCO_3$ Obtained under Different Conditions[a]

sample no.	[bmim]-[Cl] (mL)	distilled water (mL)	morphologies	size (nm)
S-0	0	15	irregular microspheres	~5000
S-1	0.2	14.8	irregular microspheres	~2000
S-2	2	13	uniform microspheres	~1500
S-3	5	10	microspheres (main)	~1500
			microcubes (little)	~1000
S-4	8	7	microspheres and microcubes	~1000
S-5	10	5	nanocubes (main)	~700
			microspheres (little)	~1000
S-6	12	3	nanocubes	~200
S-7	14	1	irregular nanoparticles	

[a] All the reactions were conducted at 120 °C for 12 h.

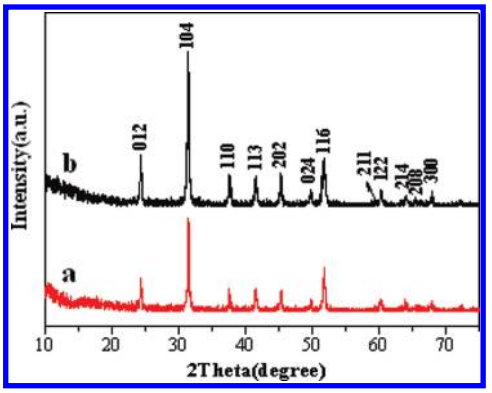

Figure 1. XRD patterns of as-synthesized samples with different morphologies: (a) S-6, $MnCO_3$ nanocubes; (b) S-2, $MnCO_3$ microsperes.

3.2. Morphology Characterization. The panoramic morphologies of the as-synthesized of $MnCO_3$ hollow microspheres are examined by SEM and TEM, as shown in Figure 2. Figure 2a is a low-magnification SEM image of the sample, which indicates that the product is composed of large-scale microspheres. Most of the micropheres exhibit monodispersive characteristics, although a few microspheres are attached to each other to form large microsphere aggregates. Figure 2b shows a typical individual $MnCO_3$ microsphere with a diameter of 1.5 μm, exhibiting the detailed structure information of the microspheres. The peripheral of the microsphere is not smooth, which is actually composed of hundreds of nanoblocks with side length of about 10 nm. From the high-magnification SEM image (Figure 2c), the microspheres have a diameter distribution ranging from 1.2 to 1.8 μm, with an average diameter of 1.5 μm. Figure 2d shows a low-magnification SEM image of broken $MnCO_3$ hollow microspheres. A few imperfect or hemispherical hollow spheres are found as arrowed, thus indicating the hollow structure of the nanospheres. Figure 2e shows the high-magnification SEM image of a broken $MnCO_3$ hollow microsphere. A cavity is observed clearly in the center of the microsphere, which provides direct evidence that the $MnCO_3$ microspheres have a hollow structure. A typical

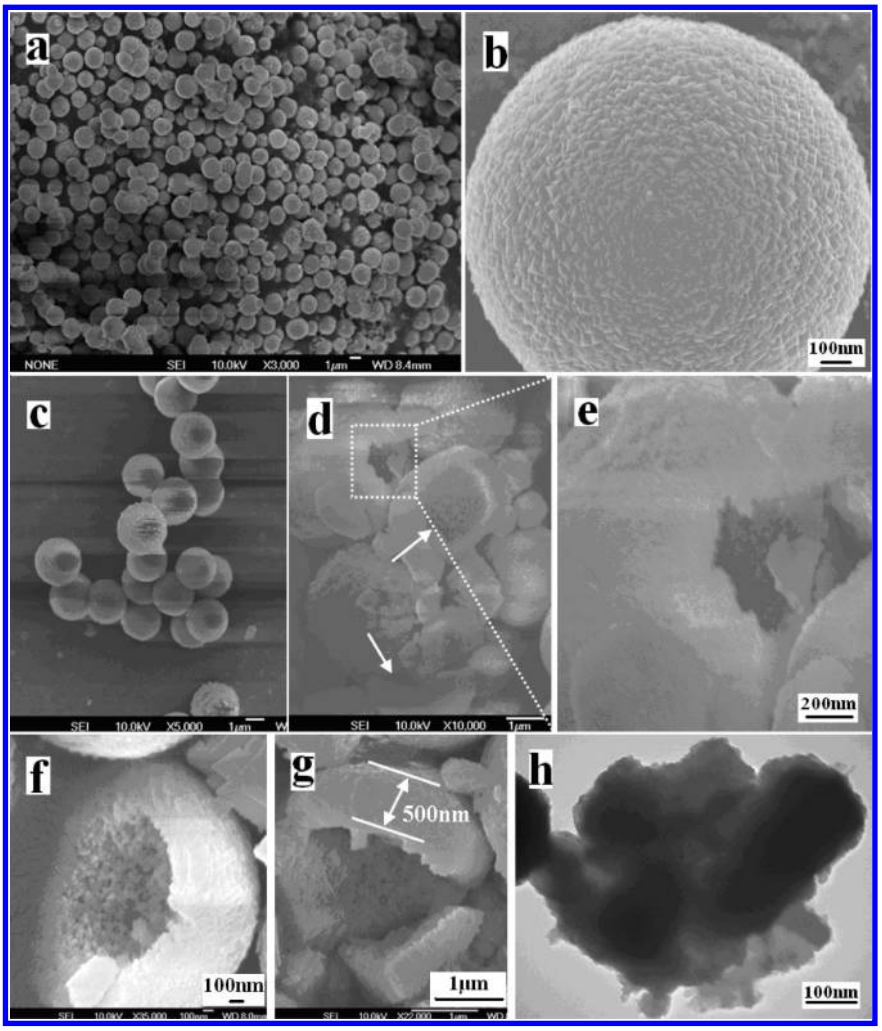

Figure 2. (a) Low- and (c) high-magnification SEM images of the as-synthesized $MnCO_3$ hollow microspheres; (b) intact $MnCO_3$ microspheres; (d) low- and (e) high-magnification SEM images of the broken $MnCO_3$ hollow microspheres. (f,g) SEM images of the shell of broken $MnCO_3$ microspheres; (f) TEM image of the shell of broken $MnCO_3$ hollow microspheres.

broken $MnCO_3$ hemisphere is shown in the Figure 2f, which further demonstrates that the shell is composed of numerous tiny nanocrystals. The shell thickness is examined by SEM and TEM, as shown in parts g and h of Figure 2, respectively. It is obviously that the shell thickness of $MnCO_3$ hollow microspheres is about 500 nm, and the diameter of hollow interiors is estimated to be about 500 nm.

The panoramic morphologies of the as-synthesized of $MnCO_3$ nanocubes are examined by SEM and TEM, as shown in Figure 3. Figure 3a shows a low-magnification SEM image of the sample, which is composed of many uniform nanocubes with side lengths of approximately 200 nm. From the high-magnification SEM image (Figure 3b), the surfaces of the nanocubes are not smooth, which is actually composed of numerous nanoplates. To further examine the surface morphology of the nanocubes, TEM images were recorded, as shown in Figure 3c,d. From the high-magnification TEM image (Figure 3d), it can be clearly found the layered structures from the edge of the cubes. The structures are actually composed of numerous nanoplates that are ordered arranged to form a cubic structure. The building blocks, 2D anisotropic $MnCO_3$ nanoplates, are about 10 nm in thickness and 200 nm in the planar dimensions.

3.3. Possible Formation Mechanism of the $MnCO_3$ Hollow Microspheres. To explore the formation mechanism of the $MnCO_3$ hollow microspheres assembled by nanoblocks, we performed several experiments that involved intercepting the intermediates at different reaction times to investigate the morphological evolution process of hollow microspheres (Figure S2 of Supporting Information).

In a typical synthesis, the formation of $MnCO_3$ microcrystals can be described by the following steps:

$$NH_4^+ + H_2O \leftrightarrow NH_3 \cdot H_2O + H^+$$

$$HCO_3^- \leftrightarrow CO_3^{2-} + H^+$$

$$Mn^{2+} + CO_3^{2-} \rightarrow MnCO_3$$

Generally, the growth process of crystals can be separated into two steps, an initial nucleating stage and a subsequent crystal growth process. At the initial nucleating stage, the crystalline phase of the seeds is critical for directing the intrinsic shapes of the crystals due to its characteristic symmetry and structure. At the subsequent step, the crystal growth stage strongly governs the final architecture of the crystals through the delicate balance between the kinetic growth and thermodynamic growth regimes.

During the nucleation stage, the initial $MnCO_3$ nuclei tended to be nanoblocks owing to the crystal nature of

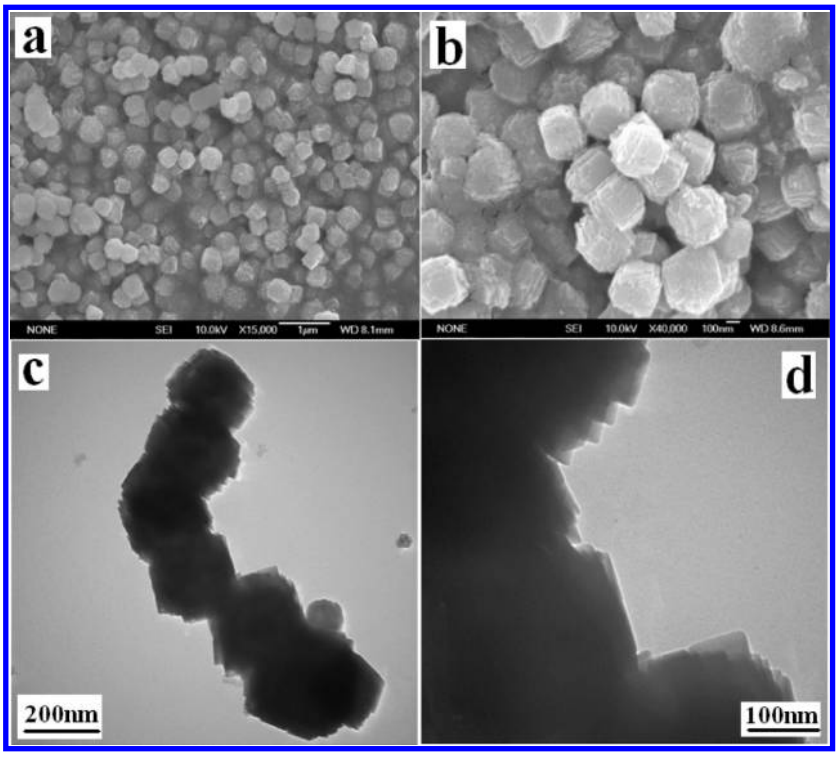

Figure 3. (a) Low- and (b) high-magnification SEM images of the as-synthesized $MnCO_3$ nanocubes; (c) low- and (d) high-magnification TEM images of the as-synthesized $MnCO_3$ nanocubes.

Scheme 2. Schematic Illustration for the Growth Process of the $MnCO_3$ Hollow Microspheres and $MnCO_3$ Nanocubes

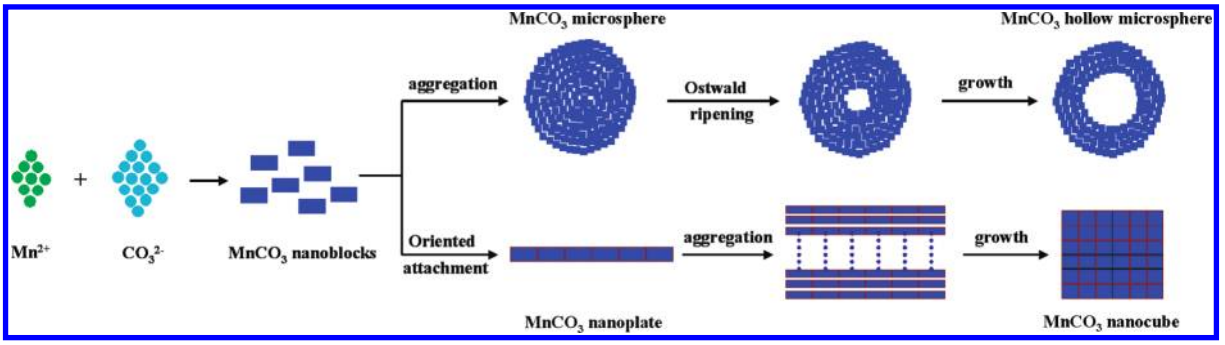

rhombohedral structure. Because of reduced surface-to-volume ratio and thus surface energy, the initial nuclei aggregated in self-assembly and quickly to be a spherical structure because a sphere possesses the highest degree of symmetry compared with other possible geometric structures. Because of the very fast nucleation, the aggregation process could be within a very short period of reaction time. In this process, nanoblocks located in the central part of the aggregate were believed to be smaller, as the nanoblocks in the shell were growing at the same time. Owing to the size difference of the forming nanocrystals, previous studies have demonstrated that the Ostwald ripening process will happen during this time because smaller, less crystalline, or less dense particles in a colloidal aggregate will be dissolved gradually while larger, better crystallized, or denser particles in the same aggregate grow.[16] During this ripening process, the inter nanoparticles would dissolve and transfer out, producing channels connecting the inner and outer spaces in the $MnCO_3$ shells. Herein, we speculated the Ostwald ripening would be accelerated in the presence of H^+ (as shown in the equation), which could form H_2CO_3 when the smaller $MnCO_3$ nanoparticles redissolved in the solution to offer CO_3^{2-} (Scheme 2). The presence of relatively abundant H_2CO_3 enhanced the degree of dissolution and the existence of a diffusion pathway through the outer crystalline shell resulted in the mesoporous structure, which was similar to our previous results for the formation of α-Fe_2O_3 nanocrystals.[7]

As a result, transformation occurs with retention of the bulk morphology by localized Ostwald ripening in which preferential dissolution of the particle interior was coupled to the deposition of a porous external shell of loosely packed nanocrystals. The cores could be further excavated with enough ripening time owing to the higher surface energy. Once the cores in the center of the microspheres are consumed completely, the hollow microspheres are formed. The [bmim][Cl] mainly plays its role subsequently by the hydrogen bonds adsorption on the surface of the nanoparticles and protecting the exteriors of the microspheres; we[6−8,20] and others[5,21] have demonstrated the synthesis of nanostructures by ionic liquid assisted route, and the electrostatic attractions mechanism is helpful to understand the influence of ionic liquids on the size control of nanostructures. As is

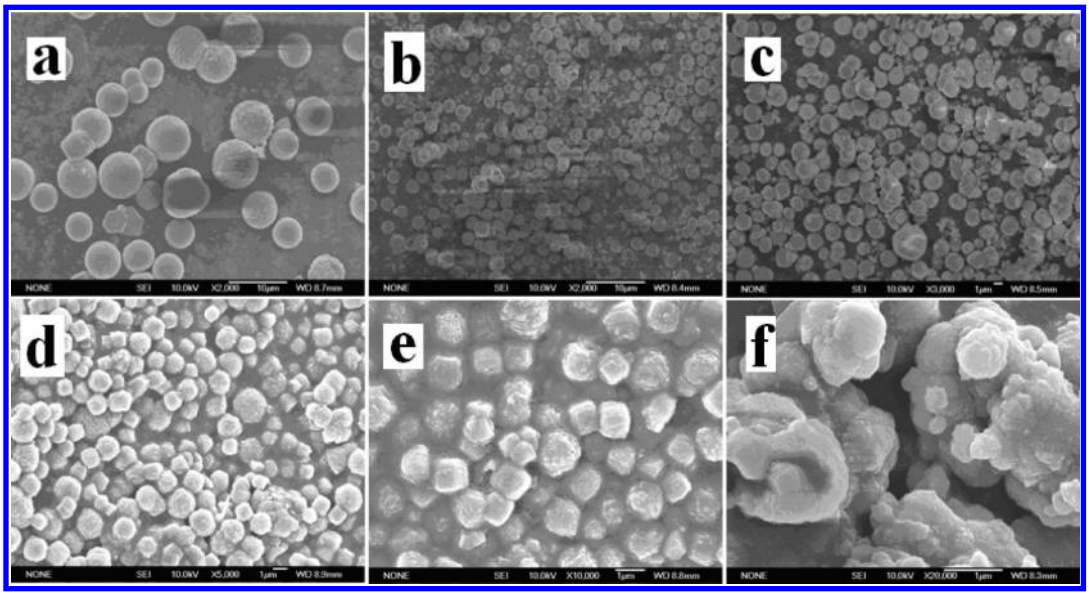

Figure 4. SEM images of the $MnCO_3$ products prepared in the presence of different concentrations of [bmim][Cl]: (a) 0 mL, (b) 0.2 mL, (c) 5 mL, (d) 8 mL, (e) 10 mL, and (f) 14 mL.

well-known, $[bmim]^+$ ions have large steric hindrance, which would hinder the agglomeration of the obtained $MnCO_3$ microspheres in the solution and accordingly the smaller $MnCO_3$ microspheres can be improved.

3.4. Effect of the [bmim][Cl] on the Formation of the $MnCO_3$ with Different Morphologies. To investigate the effect of the ionic liquid [bmim][Cl] on the formation of $MnCO_3$ with various morphologies, two controlled experiments were further carried out. The first experiment was carried out in the case of [bmim][Cl] replaced by hexadecyl trimethyl ammonium bromide (CTAB), with other experimental conditions remaining the same. As is well-known, CTAB, as a common surfactant, is widely used in the synthesis of inorganic nanomaterials as a capping agent.[22] We obtained $MnCO_3$ microspheres with an average diameter of 1.5 μm under low concentration of CTAB (Figure S3a−d of Supporting Information) and amorphous $MnCO_3$ blocks formed by irregular aggregation of small particles under high concentration of CTAB (Figure S3f of Supporting Information). The other experiment was carried out in the different concentrations of [bmim][Cl], and we obtained $MnCO_3$ crystals with different sizes and morphologies (Table 1).

These controlled experimental results indicate that the concentration of the ionic liquid plays a crucial role on the sizes and morphologies of the $MnCO_3$ crystals. We consider that the possible reasons mainly involve some aspects.

(i) In the absence of [bmim][Cl] or CTAB, we obtained nonuniformity $MnCO_3$ microspheres with a diameter distribution ranging from 4 to 8 μm (Figure 4a).

(ii) In the presence of a small amount of [bmim][Cl] (Figure 4b,c) or CTAB (Figure S3a−d of Supporting Information), we obtained with both uniformity $MnCO_3$ microspheres with an average diameter of 1.5 μm. Herein, we consider that a small amount of [bmim][Cl] can effectively control the reunion of the nanoparticles and well improve the dispersion in the reaction system just like a simple surfactant, as the same role of CTAB. Because the surfactants can cap the surface of the nanocrystals, it provides several advantages such as low agglomeration tendency, good dispersibility, and the potential to tailor the surface properties.

(iii) With increasing the concentration of CTAB, we obtained amorphous $MnCO_3$ blocks formed by irregular aggregation of small particles due to the increased viscosity of the medium (Figure S3e,f of Supporting Information). However, when the amount of the [bmim][Cl] increased, we obtained the $MnCO_3$ nanocubes (Figure 4e) with side lengths of approximately 700 nm formed by ordered aggregation of nanoplates, which was totally different from the result of CTAB. When the amount of the [bmim][Cl] increased to 12 mL, the uniform $MnCO_3$ nanocubes with side lengths of approximately 200 nm were obtained (Figure 3). Therefore, in the work reported here, the presence of the [bmim][Cl] was believed to play a strategic role on the formation of the self-assembled $MnCO_3$ nanocubes as a soft template, which is due to the important advantage of ILs that can form extended hydrogen bond systems in the liquid state and are therefore highly structured. TEM and HRTEM were employed to further reveal the formation of the $MnCO_3$ nanocubes. Figure 5a obviously shows the layered structures of the $MnCO_3$ nanocubes. From the corresponding HRTEM images (Figure 5b,c), we can see the clear lattice fringes and the interplane distances is calculated as 0.28 nm, corresponding to (104) crystal planes of rhombohedral $MnCO_3$. As is well-known, the (104) planes of $MnCO_3$ are formed by manganese atoms and carbon atoms bridged by oxygen atoms (Figure 5d, Figure S4 of Supporting Information).[23] According to our previous work,[6−8] the cations of ionic liquid can be easily adsorbed on the surface of the O^{2-}-terminated surface by electrostatic force, and the hydrogen bond, formed between the hydrogen atom at C2 position of the imidazole ring and the bridged oxygen atoms, may act as an effective bridge to connect the O^{2-}-terminated plane of the produced nuclei of metal oxide and cations of ionic liquids

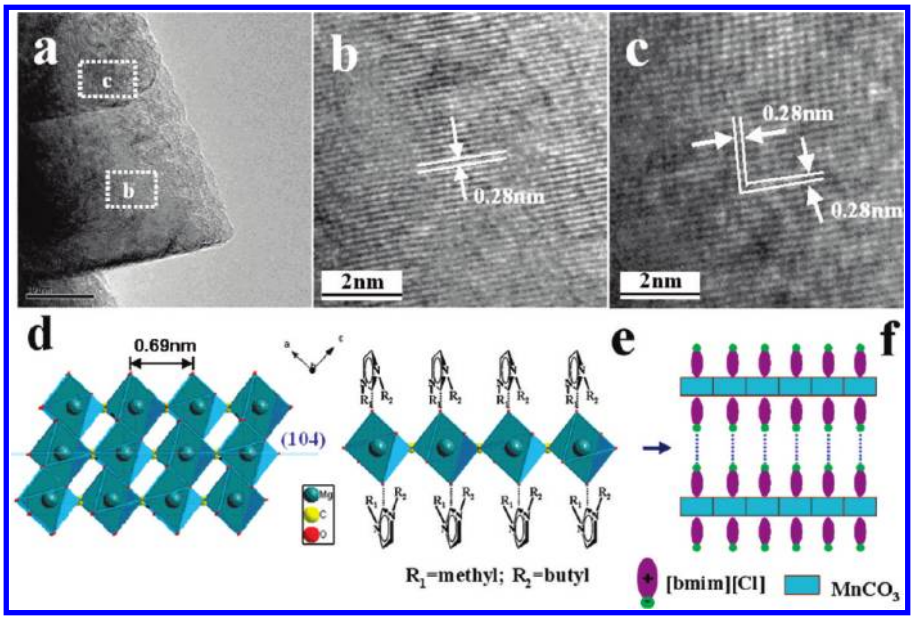

Figure 5. (a) High-magnification TEM image and (b,c) corresponding HRTEM images of the as-synthesized $MnCO_3$ nanocubes; (d) the schematic illustration of the crystal structure of rhombohedral $MnCO_3$; (e) the schematic diagram of the preferential adsorption of $[bmim]^+$ ions on the (104) plane of rhombohedral $MnCO_3$ and the hydrogen bond between the hydrogen atom at position 2 of the imidazole ring and the oxygen atom of Mn−O−C; (f) the schematic diagram of $MnCO_3$ nanocubes formed by (104) planes.

(Figure 5e). As is well-known, the $[bmim]^+$ ions are separated in accordance with the mutual π-stacking distance (0.6−0.7 nm) between the aromatic rings.[24] Fortunately, the distance between bridging O atoms above (104) plane is 0.69 nm (Figure 5d). So we suggest the $[bmim]^+$ cations will be aligned to facilitate the proposed relocation of the molecules based on its ability to self-assemble into ordered structures stabilized by additional $\pi-\pi$ interactions between the imidazolium rings of [bmim][Cl]. According to the previous studies, the hydrogen bond interaction can be investigated by FT-IR.[21a,25] As shown in Figure S1 of Supporting Information, when [bmim][Cl] is immobilized on to $MnCO_3$ blocks, the peak of the hydroxyl groups of nano-$MnCO_3$ downshifts 55 cm^{-1} (from ν_{max}/cm^{-1} 3375 to 3320), indicating a strong interaction between [bmim][Cl] and the $MnCO_3$ surface. Besides, the absorption bands at 1569, 1163, and 631 cm^{-1} in Figure S1c of Supporting Information, which was assigned to the skeleton stretching vibration of the imidazole ring, also can indicate strong interactions between [bmim][Cl] and the $MnCO_3$ surface. As a result, the (104) planes of $MnCO_3$ could be retained due to the relatively slow growth rate for the O^{2-}-terminated planes in comparison to other crystal planes, finally resulting in the self-organization of the nanoplates into the nanocubes (Figure 5f).

(iv) In addition, when the amount of [bmim][Cl] was increased to 14 mL, we obtained amorphous $MnCO_3$ blocks formed by irregular aggregation of small particles (Figure 4f). We think it may be due to the viscosity of the medium.[26] Other groups have demonstrated the viscosity of ionic liquids−water mixtures,[27] which can generally be described by the exponential expression:

$$\eta = \eta_{IL} \cdot \exp[-x_C/a]$$

where x_C is the mole fraction of water, a is a characteristic constant of the mixture, and η_{IL} is the viscosity of the pure ionic liquid. The empirical equation above indicated that the viscosity of ionic liquids−water mixtures increased exponentially when the mole fraction of water (x_C) decreased. The increasing of the [bmim][Cl] amount increased the viscosity of the system, which hindered the diffusion of monomers.

In summary, the formation processes of the $MnCO_3$ hollow microspheres and the $MnCO_3$ nanocubes can be seen in Scheme 2.

4. Conclusions

In summary, we report our recent efforts on the synthesis of $MnCO_3$ with hollow microsphere and nanocube morphologies on a lager scale using ionic liquid assisted process. We found that the sizes and morphologies of the crystals depended on the concentration of the ionic liquid. We obtained the $MnCO_3$ hollow microsphere with the low concentration of [bmim][Cl] and the $MnCO_3$ nanocubes formed by ordered aggregation of nanoplates with high concentration of [bmim][Cl]. It is believed that the $MnCO_3$ hollow microspheres are obtained by self-assembly under the driving force of Ostwald ripening process and the ionic liquid plays a crucial role on the formation of the $MnCO_3$ nanocubes. As far as our knowledge, it is rare to report the preparation of small size (~200 nm) manganese carbonate nanostructures using ionic liquids, which is highly expected that such a simple and mild route could also to be extended to prepare other metal carbonates MCO_3 (M = Sr, Ca, etc.) with small size nanostructures.

Acknowledgment. This work was supported by the National Natural of Science Foundation of China (grant no. 20971070 and 21073095) and MOE (IRT-0927) and the Project Fundamental and Applied Research of Tianjin.

Supporting Information Available: Preparation of Ionic Liquid [bmim][Cl]. This material is available free of charge via the Internet at http://pubs.acs.org.

References

(1) (a) Seddon, K. R. *Nature Mater*. **2003**, *2*, 363. (b) Welton, T. *Chem. Rev*. **1999**, *99*, 2071. (c) Adam, D. *Nature* **2000**, *407*, 938.
(2) (a) Dupont, J.; de Souza, R. F.; Suarez, P. A. Z. *Chem. Rev*. **2002**, *102*, 3667. (b) Sheldon, R. *Chem. Commun*. **2001**, *23*, 2399.
(3) (a) Buzzeo, M. C.; Evans, R. G.; Compton, R. G. *ChemPhysChem*. **2004**, *5*, 1107. (b) Huddleston, J. G.; Willauer, H. D.; Swatloski, R. P.; Visser, A. E.; Rogers, R. D. *Chem. Commun*. **1998**, *16*, 1765.
(4) (a) Blanchard, L. A.; Hancu, D.; Beckman, E. J.; Brennecke, J. F. *Nature* **1999**, *399*, 28. (b) McEwen, A. B.; McDevitt, S. F.; Koch, V. R. *J. Electrochem. Soc*. **1997**, *144*, 84. (c) Fuller, J.; Carkin, R. T.; Osteryoung, R. A. *J. Electrochem. Soc*. **1997**, *144*, 3881.
(5) (a) Dupont, J.; Fonseca, G. S.; Umpierre, A. P.; Fichtner, P. F. P.; Teixeira, S. R. *J. Am. Chem. Soc*. **2002**, *124*, 4228. (b) Endres, F.; Bukowski, M.; Hempelmann, R.; Natter, H. *Angew. Chem., Int. Ed*. **2003**, *42*, 3428. (c) Liu, D. P.; Li, G. D.; Su, Y.; Chen, J. S. *Angew. Chem., Int. Ed*. **2006**, *45*, 7370. (d) Cooper, E. R.; Andrews, C. D.; Wheatley, P. S.; Webb, P. B.; Wormald, P.; Morris, R. E. *Nature* **2004**, *430*, 1012. (e) Wang, L.; Xu, Y.; Wei, Y.; Duan, J.; Chen, A.; Wang, B.; Ma, H.; Tian, Z.; Lin, L. *J. Am. Chem. Soc*. **2006**, *128*, 7432. (f) Trewyn, B. G.; Whitman, C. M.; Lin, V. S. Y. *Nano Lett*. **2004**, *4*, 2139. (g) Cao, S. W.; Zhu, Y. J. *Acta Mater*. **2009**, *57*, 2154.
(6) Zheng, W. J.; Liu, X. D.; Yan, Z. Y.; Zhu, L. J. *ACS Nano* **2009**, *3*, 115.
(7) Lian, J. B.; Duan, X. C.; Ma, J. M.; Peng, P.; Kim, T. I.; Zheng, W. J. *ACS Nano* **2009**, *3*, 3749.
(8) Wang, L.; Chang, L. X.; Zhao, B.; Yuan, Z. Y.; Shao, G. S.; Zheng, W. J. *Inorg. Chem*. **2008**, *47*, 1443.
(9) Liu, X. D.; Ma, J. M.; Peng, P.; Zheng, W. J. *Langmuir* **2010**, *26*, 9968.
(10) Kim, T. I.; Lian, J. B.; Ma, J. M.; Duan, X. C.; Zheng, W. J. *Cryst. Growth Des*. **2010**, *10*, 2928.
(11) (a) Meldrum, F. C.; Cölfen, H. *Chem. Rev*. **2008**, *108*, 4332. (b) Li, C. C.; Yin, X. M.; Wang, T. H.; Zeng, H. C. *Chem. Mater*. **2009**, *21*, 4984. (c) Wang, W. Z.; Ao, L. *Cryst. Growth Des*. **2008**, *8*, 358. (d) Cao, J.; Zhu, Y. C.; Bao, K. Y.; Shi, L.; Liu, S. Z.; Qian, Y. T. *J. Phys. Chem. C* **2009**, *113*, 17755. (e) Cong, H. P.; Yu, S. H. *Cryst. Growth Des*. **2009**, *9*, 210.
(12) Du, J. M.; Liu, Z. M.; Li, Z. H.; Han, B. X.; Huang, Y.; Zhang, J. L. *Microporous Mesoporous Mater*. **2005**, *83*, 145.
(13) Hou, Y. W.; Kong, A. G.; Zhao, X. H.; Zhu, H. Y.; Shan, Y. K. *Mater. Lett*. **2009**, *63*, 1061.
(14) Zhao, Y.; Chen, Z. H.; Wang, H. Y.; Wang, J. J. *Cryst. Growth Des*. **2009**, *9*, 4984.
(15) Ma, Z.; Yu, J. H.; Dai, S. *Adv. Mater*. **2009**, *21*, 1.
(16) Zeng, H. C. *J. Mater. Chem*. **2006**, *16*, 649.
(17) (a) Yang, H. G.; Zeng, H. C. *J. Phys. Chem. B* **2004**, *108*, 3492. (b) Yang, H. G.; Zeng, H. C. *Angew. Chem., Int. Ed*. **2004**, *43*, 5206. (c) Liu, B.; Zeng, H. C. *Small* **2005**, *1*, 566. (d) Li, J.; Zeng, H. C. *J. Am. Chem. Soc*. **2007**, *129*, 15839–15847.
(18) Hasan, M.; Kozhevnikov, I. V.; Siddiqui, M. R. H.; Steiner, A.; Winterton, N. *Inorg. Chem*. **1999**, *38*, 5637.
(19) (a) Ehlsissen, K. T.; Delahaya-Vidal, A.; Genin, P.; Figlarz, M.; Willmann, P. *J. Mater. Chem*. **1993**, *3*, 883. (b) Tatzber, M.; Stemmer, M.; Spiegel, H.; Katzlberger, C.; Haberhauer, G.; Gerzabek, M. H. *Envoron. Chem. Lett*. **2007**, *5*, 9.
(20) Lian, J. B.; Kim, T.; Liu, X. D.; Ma, J. M.; Zheng, W. J. *J. Phys. Chem. C* **2009**, *113*, 9135.
(21) (a) Zhou, Y.; Schattka, J. H.; Antonietti, M. *Nano Lett*. **2004**, *4*, 477. (b) Zhou, Y.; Antonietti, M. *J. Am. Chem. Soc*. **2003**, *125*, 14960. (c) Taubert, A. *Angew. Chem., Int. Ed*. **2004**, *43*, 5380. (d) Nakashima, T.; Kimizuka, N. *J. Am. Chem. Soc*. **2003**, *125*, 6386. (e) Kaper, H.; Endres, F.; Djerdj, I.; Antonietti, M.; Smarsly, B. M.; Maier, J.; Hu, Y. S. *Small* **2007**, *10*, 1753.
(22) (a) Yang, S. C.; Hong, F.; Wang, L. Q.; Guo, S. W.; Song, X. P.; Ding, B. J.; Yang, Z. M. *J. Phys. Chem. C* **2010**, *114*, 203. (b) Smith, D. K.; Miller, N. R.; Korgel, B. A. *Langmuir* **2009**, *25*, 9518. (c) Kawamura, G.; Yang, Y.; Nogami, M. *J. Phys. Chem. C* **2008**, *112*, 10632.
(23) Pérez-Garridoa, C.; Astillerosa, J. M.; Fernández-Díaza, L.; Prietob, M. *J. Cryst. Growth* **2009**, *311*, 4730.
(24) (a) Yaghi, O. M.; Li, G. M.; Li, H. L. *Nature* **1995**, *378*, 703. (b) Jin, J.; Iyoda, T.; Cao, C.; Song, Y.; Jiang, L.; Li, T.; Zhu, D. *Angew. Chem., Int. Ed*. **2001**, *40*, 2135.
(25) Liu, Y. S.; Wu, G. Z.; Fu, H. Y.; Jiang, Z.; Chen, S. M.; Sha, M. L. *Dalton Trans*. **2010**, *39*, 3190.
(26) (a) Wu, L. Y.; Lian, J. B.; Sun, G. X.; Kong, X. R.; Zheng, W. J. *Eur. J. Inorg. Chem*. **2009**, *20*, 2897. (b) Lu, J.; Jiao, X. L.; Chen, D. R.; Li, W. *J. Phys. Chem. C* **2009**, *113*, 4012.
(27) (a) Comminges, C.; Barhdadi, R.; Laurent, M.; Troupel, M. *J. Chem. Eng. Data* **2006**, *51*, 680. (b) Wang, J. J.; Tian, Y.; Zhao, Y.; Zhuo, K. L. *Green Chem*. **2003**, *5*, 618.